Growth, structure, and magnetic properties of epitaxial Ni_xMn_{100-x} single layers and Co/Ni_xMn_{100-x} bilayers on $Cu_3Au(100)$

W. A. A. Macedo,* P. L. Gastelois, and M. D. Martins
Serviço de Nanotecnologia, Centro de Desenvolvimento da Tecnologia Nuclear, 31270-901 Belo Horizonte, MG, Brazil

W. Kuch, J. Miguel,† and M. Y. Khan
Institut für Experimentalphysik, Freie Universität Berlin, 14195 Berlin, Germany
(Received 18 August 2010; published 14 October 2010)

The growth and structure of single-crystalline ultrathin Ni_xMn_{100-x} films on $Cu_3Au(100)$, and also the magnetic properties of Co ultrathin films on $Ni_xMn_{100-x}/Cu_3Au(100)$ have been investigated by x-ray photoelectron and Auger electron spectroscopy, low-energy electron diffraction, reflection high-energy electron diffraction, and magneto-optical Kerr effect (MOKE). For the investigated concentration range ($10 \leq x \leq 77$), our results reveal good epitaxial layer-by-layer growth at a substrate temperature of 300 K. A weak $c(2\times2)$ superstructure was observed at the surface of all NiMn films. The average perpendicular interlayer spacing of the NiMn alloy films decreases from 1.88 Å at $x=10$ to 1.69 Å at $x=77$. The lattice parameters of equiatomic NiMn films were determined to be 3.52 Å perpendicular to the sample surface and 3.76 Å in the sample plane, indicating a face-centered tetragonal (fct) structure as expected for the $L1_0$ NiMn phase with the c axis along the film normal ("c-axis growth"). For the Co/NiMn bilayers ($23 \leq x \leq 55$), MOKE hysteresis loops show a thickness-independent coercivity, suggesting no magnetic coupling at the Co/NiMn interface. Although the structural results indicate the formation of fct NiMn in the equiatomic concentration range, we have no indication of antiferromagnetism for the NiMn films epitaxially grown on $Cu_3Au(100)$ at room temperature. This is contrary to the observations on $Co/Ni_{50}Mn_{50}$ bilayers on Cu(100), where "a-axis growth" of NiMn occurs.

DOI: 10.1103/PhysRevB.82.134423 PACS number(s): 75.70.Ak, 75.50.Ee, 68.55.−a

I. INTRODUCTION

Exchange bias (EB), originating from the interface coupling between a ferromagnet (FM) and an antiferromagnet (AFM), gives rise to shifted hysteresis loops along the magnetic field axis.[1–3] This effect, discovered more than 50 years ago,[1] is used nowadays to set a reference magnetization direction in thin-film spin-valve devices and, therefore, is of great interest for a broad range of applications based on spintronics.[4,5] Despite the enormous technological impact and the intense research efforts, one of the main challenges to understand the microscopic mechanisms of EB is the investigation of the magnetic structure at the FM/AFM interface. Moreover, unresolved issues in exchange bias include the dependence of EB effect on the crystallographic orientation of the AFM in contact with the FM, and on the chemical ordering. Also, interdiffusion at the FM/AFM interface can be particularly important for some alloy-based EB systems. In this aspect, EB systems obtained from good quality epitaxial samples could give access to well-controlled FM/AFM interfaces.

EB systems containing antiferromagnets with Néel temperatures (T_N) far above room temperature are of high importance for practical applications, and in this case the Mn-based binary alloys such as FeMn, IrMn, PdMn, PtMn, and NiMn (Refs. 2 and 4) are particularly relevant because of their excellent corrosion resistance and large bias fields. The face-centered cubic (fcc) FeMn and IrMn phases have Néel temperatures of 490 and 690 K, respectively, and the preparation of such alloys as thin films does not require any postdeposition annealing procedures.[6,7] In contrast, the AFM PdMn, PtMn, and NiMn are chemically ordered face-centered tetragonal (fct) $L1_0$ (CuAu I) phases, and the preparation of these alloys as thin films requires, often, postdeposition annealing.[8–10] In this manner, the magnetic properties of nanostructures based on these alloys depend strongly on the thermal history of the samples.

Among the technologically relevant AFM Mn-based alloys, NiMn is specially interesting due to the high thermal stability and corrosion resistance, and the highest T_N (1070 K).[11–13] Chemically ordered "equiatomic" NiMn (~45–56 at. % Ni) shows a $L1_0$ structure with lattice parameters $a=b=3.74$ Å and $c=3.52$ Å, with alternating atomic planes of Ni and Mn along the c axis, and a contraction perpendicular to these planes.[14,15] The AF I-type spin structure of $L1_0$ NiMn is characterized by an antiparallel alignment of the magnetic moments of nearest-neighbor Mn atoms. The spin axis is oriented normal to the c axis of the fct lattice.[16–19]

The preparation of equiatomic NiMn films with $L1_0$ structure is not trivial. Often this requires long postdeposition annealing procedures to induce chemical ordering, heat treatments that may result in strong interdiffusion at the FM/AFM interface and, therefore, in a complex thermal treatment-dependent magnetic behavior.[8–12] For films grown by sputtering, annealing up to 40 h at 280 °C is necessary to induce chemical ordering.[9] In this sense, since EB is an interface effect, the study of EB systems based on FM/AFM bilayers prepared starting from spontaneously ordered $L1_0$ NiMn films obtained by epitaxial growth is of strong interest.

Recent studies show that chemically ordered equiatomic NiMn can be grown epitaxially on Cu(111),[20] as well as on

Cu(100).[21–23] In the case of Cu(111), chemical order was obtained only after magnetic annealing at 250 °C and 250 Oe for 16 h, resulting in strongly temperature-dependent interface effects: a 35 Å thick interdiffused layer at the interface, and a complex behavior of the exchange bias field with temperature for Ni/NiMn bilayers on Cu(111).[20] Tieg *et al.* proposed for equiatomic $c(2\times2)$ NiMn/Cu(001) a bulklike $L1_0$ crystal structure, which is characterized by an in-plane orientation of the bulk *c* axis ("*a*-axis growth").[21] They show that Co grows layer by layer and adopts a $p(1\times1)$ structure on equiatomic $c(2\times2)$ NiMn/Cu(001). Using Co/Cu(001) as a substrate for equiatomic NiMn leads to a three-dimensional growth of the alloy film and a diffuse low-energy electron diffraction (LEED) pattern with weak $c(2\times2)$ spots. For such bilayer structures, magneto-optical Kerr effect (MOKE) measurements indicate the presence of AFM order in Ni_xMn_{100-x} films with *x* close to the equiatomic composition and thicknesses above 8 atomic monolayers (ML) at 300 K, as concluded from the Co coercivity enhancement.[21] These findings were confirmed by Reinhardt *et al.*,[22] who also found evidence of AFM order, and therefore magnetic coupling, not only in equiatomic NiMn layers with high structural quality but even for nonepitaxially grown NiMn films, and for Ni content $5<x<50$.[22]

Spin-resolved scanning tunneling microscopy results for equiatomic NiMn films on Cu(100) indicate for the $Ni_{50}Mn_{50}$(100) surface a noncollinear spin density due to reconstruction, instead of the expected ideal unreconstructed collinear spin structure. Moreover, in contrast to bulk $L1_0$ NiMn, the Ni surface atoms show a nonzero magnetic moment. The authors speculate also that the complex behavior found in NiMn could also show up at surfaces of other antiferromagnetic alloys.[23]

The dependence of EB on different crystallographic orientations of the AFM in the same FM/AFM system is an open issue in exchange bias. In the case of MnPd, one of the high Néel temperature $L1_0$ AFM model systems, different works have shown that MnPd(001) can be grown epitaxially with either the *c* axis or the *a* axis along the film normal (*c*-axis or *a*-axis growth, respectively), depending on the substrate, growth temperature, or surface morphology.[24–26] For $L1_0$ NiMn, while the use of Cu(100) as substrate leads to an *a*-axis epitaxy,[21–23] the use of Cu_3Au(100) as substrate may lead to *c*-axis epitaxy since Cu_3Au has a lattice constant $a=3.75$ Å,[27] a value that matches the lattice constant of $Ni_{50}Mn_{50}$ along the *a* axis.[14] Such an approach could possibly allow for the study of the influence of different crystallographic orientations (and also different spin structures relative to the film surface) on the magnetic coupling at the interface for the same EB system.

In this work, we investigate the growth and structure of single-crystalline Ni_xMn_{100-x} (NiMn) films, with $10\leq x\leq77$, deposited on a Cu_3Au(100) single crystal, and also the magnetism of Co layers deposited on NiMn/Cu_3Au(100) ultrathin films. For the Co/NiMn bilayers, we have focused our attention on equiatomic NiMn (where "equiatomic NiMn" means $45\leq x\leq55$, the bulk $L1_0$ NiMn concentration range), although a few samples with Ni content $x<45$ were also investigated. The films (bilayers) were prepared by codeposition (deposition) of Ni and Mn (Co) under molecular-beam epitaxy (MBE) conditions. The magnetism of Co wedges on top of thick NiMn films (12 ML) and also of thick Co films (12 ML) on top of NiMn wedges were investigated at temperatures ranging from 190 to 300 K.

II. EXPERIMENTAL ASPECTS

All the experiments were carried out in an ultrahigh vacuum (UHV) system equipped with standard techniques for preparation and analysis of thin films and surfaces including electron-beam evaporators, quartz microbalance for thickness monitoring, residual gas analyzer, x-ray photoelectron spectroscopy (XPS), and Auger electron spectroscopy (AES), LEED, and reflection high-energy electron diffraction (RHEED) to follow and characterize the film growth and thickness. The UHV system is also equipped with instruments for *in situ* MOKE magnetometry in the longitudinal geometry by using a diode laser of 670 nm wavelength and a rotatable electromagnet. The base pressure in the chamber was better than 2×10^{-10} mbar. The Cu_3Au(100) single crystal was prepared by cycles of sputtering with Ar^+ ions of 1 keV and annealing at 500 °C for about 30 min. This preparation procedure was repeated until a clean and well-ordered surface was obtained, as confirmed by AES and LEED.

The films were grown by codeposition (deposition) of Ni and Mn (Co) of high purity (Ni, Co: 99.99%, Mn: 99.95%) under MBE conditions at a typical deposition rate of 1–2 ML/min and with the substrate kept at room temperature (RT). The alloy film composition was varied by adjusting the individual deposition rates. The typical pressure during deposition was 5×10^{-10} mbar.

The composition and cleanliness of the samples were investigated by XPS and AES, and the film structure was probed by LEED and RHEED. As already mentioned, we have prepared single-crystalline ultrathin NiMn films and also Co/NiMn bilayers. The investigated bilayers were either Co films of different thickness up to 20 ML on top of NiMn continuous or stepped wedges up to 15 ML thickness, or Co wedges (7–17 ML) deposited on top of homogeneous, NiMn layers of up to 13 ML thickness. The wedge samples were always 8 mm long, allowing thickness-dependent measurements.

RHEED with a primary electron beam energy of 15 keV was employed to monitor the epitaxial growth. The Cu_3Au(100) substrate was aligned to grazing incidence of the electron beam with the [110] in-plane direction oriented parallel to the plane of incidence. The structure of the deposited films was also investigated by intensity measurements of the LEED specular beam versus electron energy [$I(V)$ curves]. The growth rate, always around 2 ML/min, was determined from the period of the RHEED oscillations. The film's lattice spacing along the surface normal was obtained from a kinematic analysis of LEED $I(V)$ curves of the (00) LEED spot, as described in Ref. 28. The LEED $I(V)$ curves were measured at an inclination angle of ~5° with respect to the sample normal.

The magnetic properties of the Co/NiMn bilayers were studied by MOKE in the longitudinal geometry. The MOKE measurements were conducted *in situ*, in UHV conditions

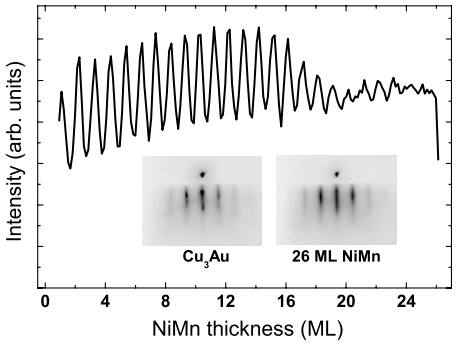

FIG. 1. RHEED oscillations for an equiatomic NiMn film 26 ML thick deposited on $Cu_3Au(100)$ at room temperature. Insets show diffraction patterns along the [110] direction for the clean substrate (left) and for 26 ML NiMn (right).

and at different temperatures, in a setup with enough sensitivity to detect magnetization of 1 ML Fe.[29] The maximum magnetic field at the sample, corresponding to a current of 5 A applied to the electromagnet inside the chamber, is limited to ~800 Oe (~63 kA/m), and the lowest sample temperature obtained by flowing liquid nitrogen through the sample manipulator was ~190 K. A field-cooling procedure to induce EB was not applied to our samples.

III. RESULTS AND DISCUSSION

The growth mode of the Ni_xMn_{100-x} layers on top of $Cu_3Au(100)$ at 300 K was investigated by RHEED. Our results for the specular RHEED intensity as a function of the deposition time (Fig. 1) show clear periodic oscillations, signature of an epitaxial, layer-by-layer growth, for the first sixteen monolayers, and then the amplitude of oscillation decreases to smaller values. The strong reduction in the amplitude of oscillation indicate the onset of the simultaneous growth of several layers (three-dimensional growth mode), as already observed for Mn-rich Ni-Mn on Cu(100),[21] and for Ni-rich Co–Ni on $Cu_3Au(100)$ (Ref. 35) after the deposition of few atomic layers. As shown in Fig. 1 for an equiatomic NiMn film ($Ni_{55}Mn_{45}$), the RHEED oscillations extend up to 26 ML NiMn. RHEED patterns obtained along the [110] direction for the clean $Cu_3Au(100)$ substrate and for 26 ML NiMn are shown in the inset, left, and right, respectively.

An evaluation of our Auger data shows that ~8 ML NiMn is enough to prevent the detection of the Cu signal (at 920 eV) from the substrate. This result indicates no or only a very small interdiffusion at the NiMn/Cu_3Au interface, i.e., the absence of any significant alloying at the NiMn/CuAu interface, in agreement with previous studies on Mn/$Cu_3Au(100)$.[33] Nevertheless, this does not exclude the possibility of having Au atoms floating on top of NiMn surface.[33,37]

The evolution of the in-plane lateral spacing of an equiatomic NiMn film ($Ni_{55}Mn_{45}$) with thickness during deposition at RT was determined from the RHEED line intensity profiles, as shown in Fig. 2(a). The in-plane spacing is obtained from the distance between two adjacent diffraction streaks in the diffraction patterns. Each point in the curve

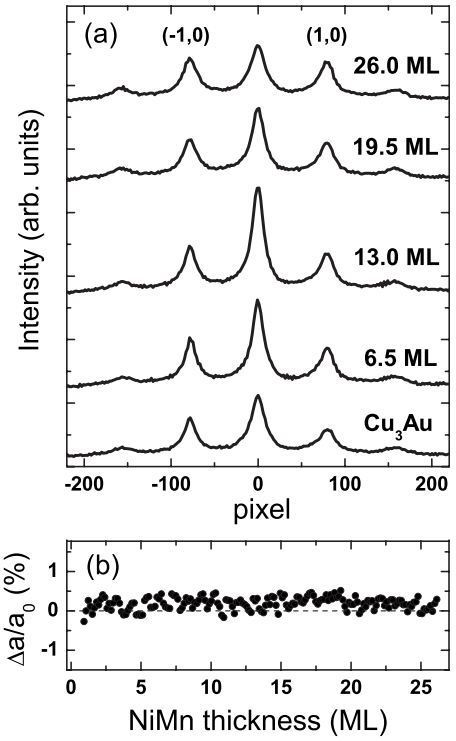

FIG. 2. (a) Intensity profiles (line scans) measured perpendicular to the RHEED patterns for the clean $Cu_3Au(100)$ substrate, and for different thicknesses of an equiatomic NiMn film grown on $Cu_3Au(100)$ at room temperature. (b) Evolution of the in-plane lattice parameter for a 26 ML thick equiatomic NiMn film, as determined from the RHEED intensity profiles. Shown is the relative variation of lattice constant a, compared to the value obtained for the $Cu_3Au(100)$ substrate (a_0) immediately prior the NiMn codeposition.

represents the relative variation of the lateral spacing in the NiMn film as compared to the lateral spacing of the $Cu_3Au(100)$ surface (3.75 Å). As can be seen in Fig. 2(b), up to at least about 26 ML (the thickest film investigated here), the lateral spacing remains constant and, within the experimental precision, identical to the lattice parameter of the $Cu_3Au(100)$ substrate. The differences in the relative intensities of the RHEED (−1,0) and (1,0) streaks observed in the line intensity profiles shown in Fig. 2(a) are equivalent for the $Cu_3Au(100)$ substrate and for 26 ML equiatomic NiMn and, therefore, should be attributed to a small misalignment of the crystal relative to the incident electron beam. They are not due to any rotation in the growth direction of the NiMn film relative to the substrate, as it is the case for Fe monolayers on Cu(100) and Cu alloy.[29–31]

Figure 3 shows the LEED patterns of the clean $Cu_3Au(100)$ substrate and of different Ni_xMn_{100-x} films deposited on $Cu_3Au(100)$ at 300 K, as indicated. The ordered $Cu_3Au(100)$ surface is characterized by the (1/2 1/2) spots of the $c(2\times2)$ superstructure, a pattern that is also observed for the Ni_xMn_{100-x} films, although with less intensity, in particular for $x=10$ and $x=28$. For NiMn, such a reconstruction is expected for a chemically ordered, bulklike, $Ni_{50}Mn_{50}(100)$ epitaxial film grown with the a axis along the film surface normal, when the Ni and Mn atoms are arranged in alternat-

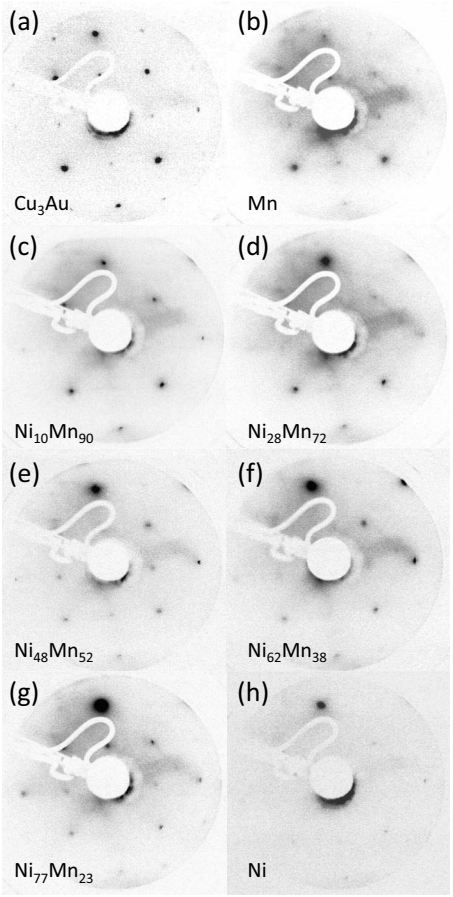

FIG. 3. LEED pictures of the $Cu_3Au(100)$ substrate and Ni_xMn_{100-x} films of different composition x on $Cu_3Au(100)$. (a) $Cu_3Au(100)$, electron energy $E=122$ eV; (b) 8.5 ML $Mn/Cu_3Au(100)$, $E=126$ eV; (c) 8.0 ML $Ni_{10}Mn_{90}/Cu_3Au(100)$, $E=120$ eV; (d) 8.2 ML $Ni_{28}Mn_{72}/Cu_3Au(100)$, $E=127$ eV; (e) 8.8 ML $Ni_{48}Mn_{52}/Cu_3Au(100)$, $E=123$ eV; (f) 6.0 ML $Ni_{62}Mn_{38}/Cu_3Au(100)$, $E=126$ eV; (g) 6.8 ML $Ni_{77}Mn_{23}/Cu_3Au(100)$, $E=121$ eV; and (h) 7.5 ML $Ni/Cu_3Au(100)$, $E=115$ eV.

ing atomic planes perpendicular to the c axis,[16] as observed for equiatomic NiMn on top of Cu(100),[21–23] but should not be the case for c-axis growth of this phase on a (100) fcc surface. The additional ordered structure at the surface of the NiMn films might just come from a reconstruction of NiMn atoms at the surface, or even be due to some Au segregation to the very first atomic layers of the NiMn surface, as already reported for thin Mn, as well as Co-Ni alloy films grown on top of $Cu_3Au(100)$.[33–35]

The presence of Au floating on top of the NiMn films was explored here by AES, from the evolution of the Ni, Mn, Cu, and Au Auger lines at low energy (~30–100 eV) with increasing NiMn thickness. The results (not shown) indicate Au segregation in the first monolayers, but 11–12 ML NiMn suppress completely the Au signal (at 69 eV). Therefore, the weak $c(2\times2)$ reconstruction at the surface NiMn films, which was still observed at thicknesses of 15 ML and more, seems not to be due to the Au atoms segregated to the very surface of NiMn on $Cu_3Au(100)$.

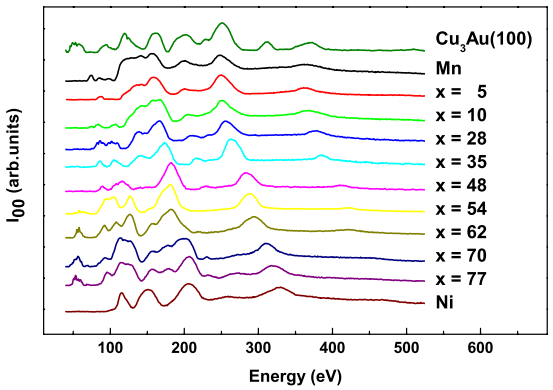

FIG. 4. (Color online) Room temperature LEED $I(V)$ curves for a series of different ~8 ML thick Ni_xMn_{100-x} films (6 ML for $x=62$) deposited on the $Cu_3Au(100)$ substrate at RT, as indicated.

The crystallographic structure of the $Ni_xMn_{100-x}/Cu_3Au(100)$ along the surface normal was determined from LEED $I(V)$ curves. Only films grown at room temperature were investigated. The (00) diffraction beam intensity curves for different NiMn films were collected at RT as a function of the electron energy [$I_{00}(V)$ curves] after film deposition, and a kinematic approximation was used to calculate the average vertical interplanar distance of the top NiMn atomic layers in the films.[36] Considering that the electrons undergo only single scattering in the diffraction process (the kinematic approximation), the vertical (perpendicular) interlayer distance d_p can be evaluated by using the expression

$$d_p = n\pi\hbar/\{[2m(E_p + V_0)]^{1/2}\sin\theta\},$$

where E_p is the primary electron energy of the Bragg peak of order n, V_0 is the additional energy shift due to the average inner potential in the crystal, m is the electron mass, and θ is the incident angle with respect to the sample surface. A linear fitting of the E_p versus n^2 points extracted from the $I(V)$ curves gives the vertical interlayer distance d_p.[36]

The LEED $I(V)$ curves for NiMn films (~8 ML thick) of different concentrations, from pure Mn to pure Ni, as deposited at room temperature, are shown in Fig. 4, where the maxima above 150 eV were identified as the fourth-, fifth-, and sixth-order Bragg maxima. The determination of the perpendicular interlayer spacing d_p from the $E(n^2)$ curves is illustrated in Fig. 5 for the $Cu_3Au(100)$ substrate and for three epitaxially grown equiatomic NiMn films, $Ni_{45}Mn_{55}$, $Ni_{52}Mn_{48}$, and $Ni_{55}Mn_{45}$, 24, 12, and 26 ML thick, respectively. The straight lines represent linear regression fittings based on the kinematic approximation of the (00) diffraction beam intensity, as described above. For all NiMn films grown with near equiatomic composition and at a substrate temperature of 300 K, the average interlayer distance perpendicular to the sample surface is contracted relative to $Cu_3Au(100)$, as evidenced by the lower slope of the $E(n^2)$ curve for the substrate. The interlayer spacings were determined to be 1.78 ± 0.02 Å for 24 ML $Ni_{45}Mn_{55}$ and 1.76 ± 0.02 Å for both the 12 ML thick $Ni_{52}Mn_{48}$ and the 28 ML thick $Ni_{55}Mn_{45}$ films.

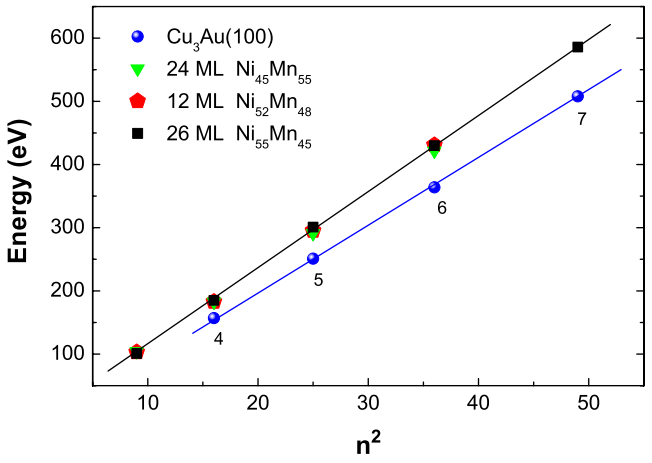

FIG. 5. (Color online) Energy dependence on n^2 for three different NiMn films near equiatomic concentration ($Ni_{45}Mn_{55}$, $Ni_{52}Mn_{48}$, and $Ni_{55}Mn_{45}$, 24, 12, and 26 ML thick, respectively) and for the $Cu_3Au(100)$ substrate. The contraction of the perpendicular interlayer distance in the NiMn films (of 5.3%) relative to the $Cu_3Au(100)$ substrate is evident. The full (blue) circles are for the Cu_3Au substrate, and the hexagons (red), squares (black), and triangles (green) are for the 24 ML $Ni_{45}Mn_{55}$, 12 ML $Ni_{52}Mn_{48}$, and 26 ML $Ni_{55}Mn_{45}$, respectively. Please note that for the NiMn films there is a strong superposition of the data points.

The average vertical interlayer spacing d_p obtained for Ni_xMn_{100-x} layers on $Cu_3Au(100)$ as a function of the Ni content x is shown in Fig. 6, where the dashed horizontal lines at 1.88 and 1.76 Å indicate the interlayer spacings in fcc $Cu_3Au(100)$, as experimentally obtained here, and in bulk $L1_0$ NiMn along the c axis, respectively. The interlayer spacing of Cu_3Au coincides with the value of bulk $L1_0$ NiMn

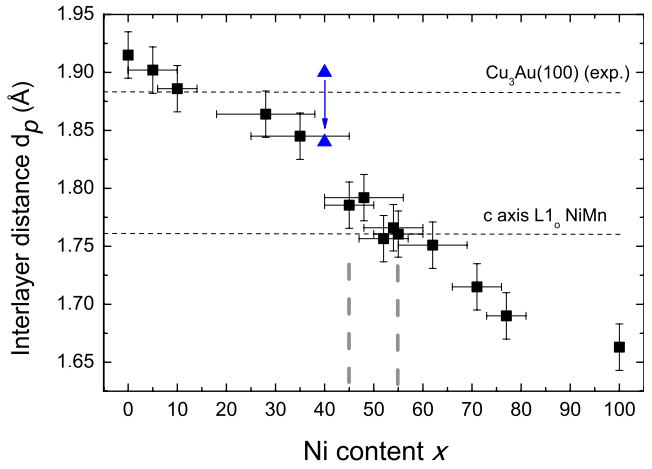

FIG. 6. (Color online) Perpendicular interlayer distance d_p vs Ni concentration in Ni_xMn_{100-x} on $Cu_3Au(100)$ at room temperature. The full triangles (blue points) limiting the arrow at $x=40$ represent the extreme values of d_p when the thickness of a $Ni_{40}Mn_{60}$ film increases from 3 to 10 ML (see text). The dashed horizontal lines at 1.88 and 1.76 Å indicate the interlayer spacings in fcc $Cu_3Au(100)$, as experimentally obtained here, and in bulk $L1_0$ NiMn along the c axis, respectively. The dashed vertical (gray) lines indicate the $L1_0$ region for bulk NiMn. Note that for equiatomic NiMn films d_p coincides with the value of the c axis in bulk $L1_0$ NiMn.

along the a axis, as already mentioned, and the spacing along c in $L1_0$ NiMn coincides with the value of bulk fcc Ni. The average interlayer spacing of the NiMn alloy films decreases from 1.88(2) Å at $x=10$ to 1.69(2) Å at $x=77$. For pure Mn ($x=0$), our value of 1.91(2) Å is in good agreement with the value obtained by Lin *et al.*[33] for RT-grown Mn films on $Cu_3Au(100)$ below 10–12 ML. For pure Ni ($x=100$), our value of 1.66(2) Å is smaller than the values of Ref. 32, indicating more strained films for equivalent thicknesses. As expected, the known tetragonal distortion of epitaxial ultrathin Ni films on Cu(001),[21–23,37] characterized by an in-plane expansion of the fcc Ni lattice and a compression along the surface normal, is also observed here, as demonstrated by the lower average interlayer spacing in comparison to bulk Ni.

We have also determined the interlayer spacing d_p as a function of the film thickness for a $Ni_{40}Mn_{60}$ wedge. As plotted in Fig. 6 for the extreme values obtained (full blue triangles), d_p is equal to 1.90 Å up to 3 ML, and then starts to relax, decreasing linearly to reach 1.85 Å at 10 ML, remaining constant at that value until 13 ML $Ni_{40}Mn_{60}$. This observation is consistent with the results of Braun *et al.* for pure Ni films on $Cu_3Au(100)$.[32] For pure Mn films on $Cu_3Au(100)$ at room temperature, Lin *et al.* observed an abrupt decrease in the interlayer distance at a critical thickness around 13 ML.[33]

This perpendicular interlayer distance corresponds to a contraction of 5.3% relative to the in-plane spacing determined by RHEED for these films, and is in good agreement with the expected value of the interlayer distance along the c-axis in bulk $L1_o$ NiMn. Having in mind that we observe an in-plane interlayer distance that matches the $Cu_3Au(100)$ substrate, i.e., a value of 1.88 ± 0.02 Å for the interlayer distance in the sample plane, our results are a clear indication of an fct structure with the c/a ratio compatible with the one expected for $L1_0$ NiMn, and with the a and b axes in plane. In contrast to equiatomic NiMn on Cu(100),[21–23] for NiMn films on $Cu_3Au(100)$ we observe a tetragonal distortion compatible with an epitaxial c-axis growth of fct NiMn(100).

The magnetic order of thick (12–26 ML), epitaxial equiatomic NiMn films on $Cu_3Au(100)$ was probed *in situ* by longitudinal MOKE measurements in UHV conditions. MOKE hysteresis loops were measured by applying the external magnetic field along the ⟨100⟩ direction, and no Kerr signal, that is, no signal of ferromagnetic order was detected at RT or even at 190 K, in agreement with the bulk NiMn phase diagram, where AFM order is expected for concentrations around equiatomic NiMn.

To address the antiferromagnetic order in the NiMn films grown on $Cu_3Au(100)$, Co layers were deposited on top of different $Ni_xMn_{100-x}/Cu_3Au(100)$ samples, and the magnetism of the Co/NiMn bilayers was checked by MOKE. In case of a FM/AFM coupling at the Co/NiMn interface, the MOKE loops for the same sample are expected to show a thickness-dependent coercivity, evidencing AFM order in NiMn, as already observed in Co/NiMn bilayers deposited on Cu(100).[21,22] For the FM Co wedges (7–17 ML) on top of sufficiently thick, AFM NiMn films, the coercivity is expected to decrease in this case with increasing Co thickness due to the interfacial nature of the FM/AFM coupling.[21,22] For bilayers of sufficiently thick Co films on top of NiMn

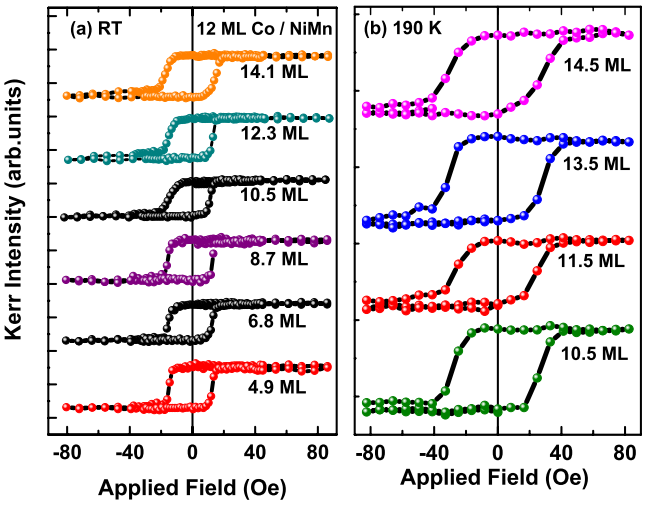

FIG. 7. (Color online) Longitudinal MOKE loops for a 12 ML thick Co film on top of an equiatomic NiMn wedge ($Ni_{54}Mn_{46}$, 4–15 ML) at (a) 300 K and (b) 190 K, and at different NiMn thicknesses, as indicated. At least the two top most loops in (a) and (b) correspond to Co/NiMn bilayers with equiatomic NiMn thickness far above the critical thickness for the onset of antiferromagnetic order at room temperature in NiMn films grown on Cu(100).

wedges, the Co coercivity is expected to increase above ~8 ML NiMn since this is the critical thickness for AFM order at room temperature for equiatomic NiMn films on Cu(100).[21,22]

Our MOKE results are shown in Figs. 7–9 for 12 and 20 ML thick Co films on top of NiMn wedges (up to 15 ML) and for a Co wedge (7–17 ML) deposited on top of a homogeneous 12 ML thick NiMn layer. They reveal an unexpected uniform magnetic behavior: almost constant coercive fields for all the positions along the wedges, i.e., at different Co and NiMn thicknesses, showing no evidence of coupling of the FM Co atoms to AFM NiMn atoms in all the Co/NiMn interfaces grown on the $Cu_3Au(100)$ single crystal.

Reinhardt *et al.*[22] showed, by changes of the coercivity in MOKE measurements, evidence of antiferromagnetic order in Ni_xMn_{100-x} alloy films on Cu(100) for $5<x<50$, which is not observed for $x=60$. Tieg *et al.*[21] explored the presence of antiferromagnetism in NiMn on Cu(100) only for alloys around equiatomic concentration, and have found AFM order for $x=50$ and $x=60$, but not for $x=65$. Taking into account that in both works the relative concentrations of Ni and Mn atoms were determined by low resolution AES, method that offers an uncertainty around ±5 at. %, these results are in reasonable agreement for the limit of AFM order in NiMn films on Cu(100) near equiatomic concentrations, but only in Ref. 22 the authors have looked for magnetic coupling in Mn-rich Co/NiMn bilayers on $Cu_3Au(100)$.

We have also searched for evidence of FM/AFM coupling in Co/NiMn bilayers on $Cu_3Au(100)$ for two Ni concentrations below the $L1_0$ range: 23 and 33 at. % Ni. As illustrated in Fig. 10 for $x=33$, MOKE loops at RT for bilayers of 6 ML Co on top of 5 and 10 ML $Ni_{33}Mn_{67}/Cu_3Au(100)$ show the same coercivity as when the Co film is deposited directly on top of the Cu_3Au substrate (0 ML). Similar to the observation for bilayers with equiatomic NiMn, no signal of FM/AFM coupling was detected for the Co/NiMn bilayers with Mn-rich films.

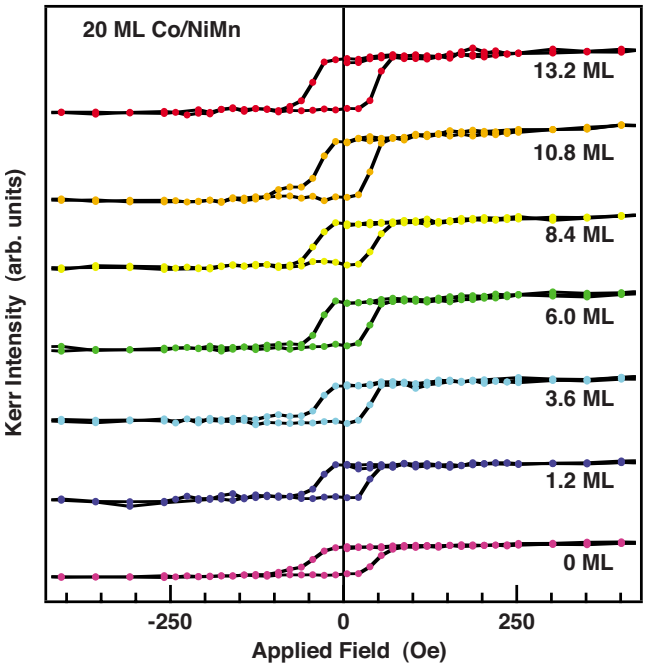

FIG. 8. (Color online) Longitudinal MOKE loops of a 20 ML thick Co film on top of an equiatomic NiMn wedge ($Ni_{48}Mn_{52}$, 0–4 ML) at 300 K. For the different loops, the NiMn thicknesses are indicated. As in Fig. 7, at least the two top most MOKE curves correspond to Co/NiMn bilayers with the NiMn thickness far above the critical one for the onset of antiferromagnetic order at room temperature in NiMn films grown on Cu(100)

In summary, we have searched for FM/AFM coupling in Co/Ni_xMn_{100-x} bilayers epitaxially grown on $Cu_3Au(100)$ at room temperature, through the evolution of Co coercivity as a function of the thickness of the different Ni_xMn_{100-x} ultrathin films. For x ranging from 23 to 55, no change in Co

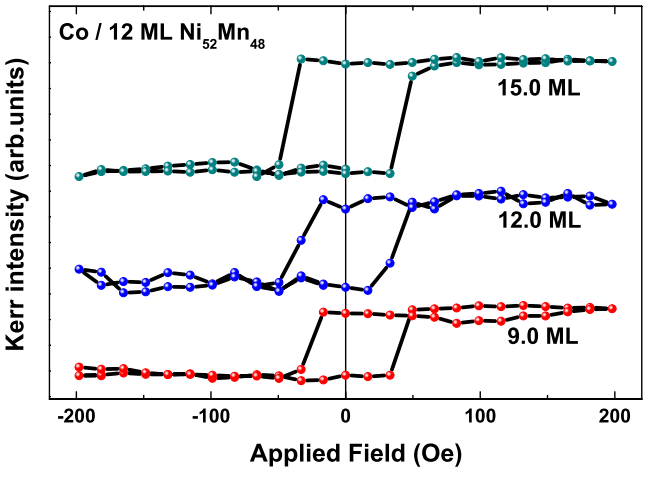

FIG. 9. (Color online) Longitudinal MOKE loops at room temperature along a thick Co wedge (7–17 ML) on top of 12 ML $Ni_{52}Mn_{48}/Cu_3Au(100)$. Please note that a small increase in the coercivity for increasing Co thickness is contrary to the expected fingerprint of AFM order in the equiatomic NiMn alloy film.

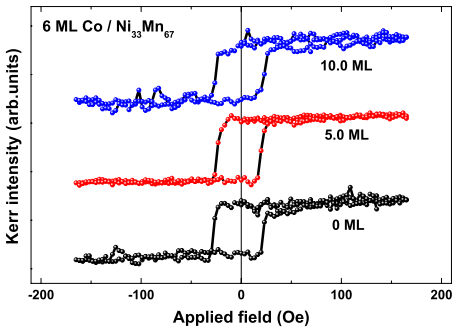

FIG. 10. (Color online) Longitudinal MOKE loops at room temperature for bilayers of 6 ML Co/n ML $Ni_{33}Mn_{67}$ on $Cu_3Au(100)$: $n=0$, $n=5$, and $n=10$ (loops along a stepped-wedge sample).

coercivity occurs for NiMn thicknesses above 8–10 ML, i.e., for NiMn films thick enough to be AFM-ordered at RT. Despite the broad NiMn concentration range covered, no evidence of magnetic coupling in the Co/NiMn interfaces deposited on $Cu_3Au(100)$ was observed in our work. Possible reasons for the absence of magnetic coupling in the Co/NiMn bilayers are the lack of sufficient chemical (i) or crystallographic (ii) order in the fct NiMn films, (iii) interdiffusion and presence of Au atoms along the NiMn layer. Also, although in bulk $L1_0$ NiMn the Mn spins are expected to be oriented normal to the c axis of the fct lattice, since for NiMn films on $Cu_3Au(100)$ we observe a 90° rotation of the growth direction when compared to NiMn/Cu(100), one could speculate that (iv) the Mn spins are completely aligned along the c axis, and thus perpendicular to the Co magnetization direction. Thermal treatment of the NiMn films would in principle improve the chemical and crystallographic order, but it would at the same time induce alloying with the substrate, very likely resulting in a larger interdiffusion with the Cu_3Au substrate.

IV. CONCLUSION

We have investigated the growth and structure of single-crystalline Ni_xMn_{100-x} ultrathin films on $Cu_3Au(100)$ and also the magnetic properties of Co monolayers on $Ni_xMn_{100-x}/Cu_3Au(100)$. For the Ni_xMn_{100-x} films ($10 \leq x \leq 77$), our results revealed good epitaxial, layer-by-layer growth at a substrate temperature of 300 K. A weak signal of a $c(2\times2)$ superstructure was observed at the surface of the NiMn films for all the investigated concentration range. The average perpendicular interlayer distance of the NiMn alloy films decreases from 1.88 Å at $x=10$ to 1.69 Å at $x=77$. The lattice parameters of equiatomic NiMn films were determined to be 3.52 Å perpendicular to the sample surface and 3.76 Å in the sample plane, indicating a fct structure as expected for the $L1_0$ NiMn phase, and with the c axis along the film normal, i.e., c-axis growth.

For the Co/NiMn bilayers on $Cu_3Au(100)$, MOKE hysteresis loops show a thickness-independent coercivity, suggesting the absence of magnetic coupling at the Co/NiMn interface for the Ni content ranging from 23 to 55 at. %. Although the structural results indicate the formation of fct NiMn for equiatomic films, we have no indication of magnetic coupling between 190 and 300 K for Co/NiMn bilayers epitaxially grown on $Cu_3Au(100)$ at room temperature. This is contrary to the observation for Co monolayers on equiatomic, a-axis grown NiMn on Cu(100). Possible reasons for the absence of increase in the coercivity at room temperature in the Co/NiMn bilayers on $Cu_3Au(100)$ could be either the absence of antiferromagnetism in the equiatomic NiMn due to some chemical and/or crystallographic disorder, or even a NiMn spin order perpendicular to the Co magnetization.

ACKNOWLEDGMENTS

Work supported by the CNPq-DFG Bilateral Cooperation on Nanotechnology, Grants No. 490420/2007-9 (Brazil) and No. 444 BRA 113/34/0-1 (Germany), by the CNPq, and by the FAPEMIG (MG, Brazil). M.Y.K. acknowledges financial support for the stay in Germany from the Kohat University of Science & Technolgy, Kohat, Pakistan.

*Corresponding author; wmacedo@cdtn.br
†Present address: Diamond Light Source Ltd., Harwell Science and Innovation Campus, Diamond House, Chilton, Didcot, Oxfordshire OX11 0DE, UK.

[1] W. H. Meiklejohn and C. P. Bean, Phys. Rev. **102**, 1413 (1956).
[2] J. Nogués and I. K. Schuller, J. Magn. Magn. Mater. **192**, 203 (1999).
[3] F. Radu and H. Zabel, in *Magnetic Heterostructures*, edited by S. D. Bader and H. Zabel (Springer, Berlin, 2007).
[4] S. S. P. Parkin, K. P. Roche, M. G. Samant, P. M. Rice, R. B. Beyers, R. E. Scheuerlein, E. J. O'Sullivan, S. L. Brown, J. Bucchigano, D. W. Abraham, Yu Lu, M. Rooks, P. L. Trouilloud, R. A. Wanner, and W. J. Gallagher, J. Appl. Phys. **85**, 5828 (1999).
[5] S. S. P. Parkin, X. Jiang, C. Kaiser, A. Panchula, K. Roche, and M. G. Samant, Proc. IEEE **91**, 661 (2003).
[6] W. Kuch, F. Offi, L. I. Chelaru, M. Kotsugi, K. Fukumoto, and J. Kirschner, Phys. Rev. B **65**, 140408(R) (2002), and references therein.
[7] M. Ali, C. H. Marrows, M. Al-Jawad, B. J. Hickey, A. Misra, U. Nowak, and K. D. Usadel, Phys. Rev. B **68**, 214420 (2003).
[8] T. Lin, D. Mauri, N. Staud, C. Hwang, J. K. Howard, and G. L. Gorman, Appl. Phys. Lett. **65**, 1183 (1994).
[9] Z. Qian, J. M. Sivertsen, J. H. Judy, B. A. Everitt, S. Mao, and E. S. Murdock, J. Appl. Phys. **85**, 6106 (1999).
[10] M. F. Toney, M. G. Samant, T. Lin, and D. Mauri, Appl. Phys. Lett. **81**, 4565 (2002).
[11] B. Dai, J. W. Cai, W. Y. Lai, F. Shen, Z. Zhang, and G. H. Yu, Appl. Phys. Lett. **82**, 3722 (2003).
[12] C. Loch, W. Maaass, B. Ocker, and K. Röll, J. Appl. Phys. **85**, 4460 (1999).
[13] E. Krén, E. Nagy, I. Nagy, L. Pál, and P. Szabó, J. Phys. Chem.

Solids **29**, 101 (1968).
[14] L. Ding, P. F. Ladwig, X. Yan, and Y. A. Chang, Appl. Phys. Lett. **80**, 1186 (2002).
[15] L. Pál, E. Krén, G. Kádár, P. Szabó, and T. Tarnóczi, J. Appl. Phys. **39**, 538 (1968).
[16] J. S. Kasper and J. S. Kouvel, J. Phys. Chem. Solids **11**, 231 (1959).
[17] D. Spišák and J. Hafner, J. Phys.: Condens. Matter **11**, 6359 (1999).
[18] V. V. Godlevsky and K. M. Rabe, Phys. Rev. B **63**, 134407 (2001).
[19] A. Sakuma, J. Magn. Magn. Mater. **187**, 105 (1998).
[20] M. S. Lund, M. R. Fitzsimmons, S. Park, and C. Leighton, Appl. Phys. Lett. **85**, 2845 (2004).
[21] C. Tieg, W. Kuch, S. G. Wang, and J. Kirschner, Phys. Rev. B **74**, 094420 (2006).
[22] M. Reinhardt, J. Seifert, M. Busch, and H. Winter, Phys. Rev. B **81**, 134433 (2010).
[23] C. L. Gao, A. Ernst, A. Winkelmann, J. Henk, W. Wulfhekel, P. Bruno, and J. Kirschner, Phys. Rev. Lett. **100**, 237203 (2008).
[24] R. F. C. Farrow, M. F. Toney, R. F. Marks, K. Hannibal, A. Kellock, A. Brooks, J. A. Borchers, and K. V. O'Donovan, Intermag, 2001 (unpublished).
[25] N. Cheng, J.-P. Ahn, and K. M. Krishnan, J. Appl. Phys. **89**, 6597 (2001).
[26] R. F. C. Farrow, R. F. Marks, M. F. Toney, S. David, A. J. Kellock, J. A. Borchers, K. V. O'Donovan, and D. Smith, Appl. Phys. Lett. **80**, 808 (2002).
[27] F. Bruno, D. Cvetkob,L. Floreano, R. Gotter, C. Mannori, L. Mattera, R. Moroni, S. Prandi, S. Terreni, A. Verdini, and M. Canepa, Appl. Surf. Sci. **162-163**, 340 (2000); W. A. A. Macedo, W. Keune, and R. D. Ellerbrock, J. Magn. Magn. Mater. **93**, 552 (1991).
[28] F. Offi, W. Kuch, and J. Kirschner, Phys. Rev. B **66**, 064419 (2002).
[29] M. D. Martins, L. H. F. Andrade, P. L. Gastelois, and W. A. A. Macedo, J. Appl. Phys. **89**, 6680 (2001).
[30] S. Müller, P. Bayer, C. Reischl, K. Heinz, B. Feldmann, H. Zillgen, and M. Wuttig, Phys. Rev. Lett. **74**, 765 (1995).
[31] H. Zillgen, B. Feldmann, and M. Wuttig, Surf. Sci. **321**, 32 (1994).
[32] A. Braun, B. Feldmann, and M. Wuttig, J. Magn. Magn. Mater. **171**, 16 (1997).
[33] W. C. Lin, T. Y. Chen, L. C. Lin, B. Y. Wang, Y. W. Liao, Ker-Jar Song, and Minn-Tsong Lin, Phys. Rev. B **75**, 054419 (2007).
[34] Y. Wang, W. C. Lin, Y. W. Liao, Ker-Jar Song, and Minn-Tsong Lin, Surf. Sci. **600**, 4517 (2006).
[35] W. C. Lin, B. Y. Wang, Y. W. Liao, Ker-Jar Song, and Minn-Tsong Lin, Phys. Rev. B **71**, 184413 (2005).
[36] J. B. Pendry, *Low Energy Electron Diffraction* (Academic, New York, 1974).
[37] B. Schirmer, B. Feldmann, A. Sokoll, Y. Gauthier, and M. Wuttig, Phys. Rev. B **60**, 5895 (1999).